Energy Advances

ROYAL SOCIETY OF CHEMISTRY

PAPER

View Article Online
View Journal

Cite this: DOI: 10.1039/d6ya00065g

Solid-state prealkylation of electrode architectures to tune solid electrolyte interphase composition†

Amanda L. Musgrove, *[a] Ankit Verma, [b] Marco-Tulio F. Rodrigues,[c] Evelyna Wang,[c] Baris Key,[c] Anton Grabo-Tomich,[c] Christopher S. Johnson, [c] Robert L. Sacci, [a] Steven Lam,[ad] Harry M. Meyer III,[a] Andrew M. Colclasure,[b] Beth L. Armstrong[e] and Gabriel M. Veith *[ad]

Efficient electrochemical cycling of certain Si anodes is limited by irreversible Li consumption to form and continually reform the solid electrolyte interface (SEI) due to Si expansion/contraction and fracture. Prelithiation can compensate for these losses; however, the starting open circuit potential (V_{OC}) becomes highly reducing and, therefore, the electrolyte reduction chemistry that influences the SEI composition can change. Herein, we compare SEI formation for electrodes prelithiated using Solid State Prealkylation of Electrode Architectures (SPEAR) *versus* traditional electrochemically lithiated architectures (ECLAR), focusing on SEI compositional changes as a function of stoichiometry ($0.28 \leq x \leq 1.38$ in Li_xSi). Increasing SPEAR prelithiation decreased the initial V_{OC} of Si anodes *vs.* Li/Li^+ from ~3 V ($Li_{0.28}Si$) to < 0.5 V for $Li_{1.38}Si$, enabling simultaneous competitive reduction of EC, EMC, and $LiPF_6$ at low potentials. *Ex situ* ^7Li and ^{29}Si cross-polarization NMR and XPS reveal that SPEAR drives thicker SEI formation with substantially increased P/F contributions and a predominantly inorganic insoluble SEI (71.4% inorganic for $Li_{1.38}Si$), consistent with accelerated $LiPF_6$-derived $PO_x/LiPF_x/LiF$ formation relative to ECLAR analogs which exhibit carbonate-rich organic SEI compositions. Symmetric-cell EIS further indicates SPEAR-specific impedance features consistent with pore reduction (filling) during Li_xSi formation. In full cells, SPEAR prelithiation increases the initial coulombic efficiency (ICE) and accelerates SEI formation and stabilization with $Li_{1.38}Si$ reaching 99.4% coulombic efficiency (CE) by cycle 2.

Received 5th March 2026,
Accepted 20th April 2026

DOI: 10.1039/d6ya00065g

rsc.li/energy-advances

1. Introduction

The electrochemical cycling of certain Si electrodes in Li-ion batteries is challenging because the initial formation of a solid electrolyte interphase (SEI) during cycling consumes 15% or more of available Li.[1,2] Additionally, electrode expansion during cycling causes SEI cracking which exposes active Si and causes unsteady, continual SEI reformation and excessive electrolyte consumption.[3,4] Si electrode prelithiation is often implemented to overcome some of these challenges, as the additional Li reservoir can compensate for irreversible Li losses. There are many approaches to prelithiation. Most focus on the electrochemically driven insertion of Li supported by liquid electrolytes.[5–8] An emerging alternative approach is the Solid State Prealkylation of Electrode Architectures, or "SPEAR" method.[9] Here, Li is evaporated in line-of-sight of the electrode surface, resulting in Li deposition at temperatures > 400 °C and enabling solid-state diffusion into the electrode bulk. The deposition is highly uniform across the electrode and has shown up to a 63% improvement in specific capacity which is attributed to increased Si utilization.[10]

[a] Chemical Sciences Division, Oak Ridge National Laboratory, Oak Ridge, Tennessee 37831, USA. E-mail: musgroveal@ornl.gov, veithgm@ornl.gov
[b] Energy Conversion and Storage Systems Center, National Laboratory of the Rockies, Golden, Colorado 80401, USA
[c] Chemical Sciences and Engineering Division, Argonne National Laboratory, Lemont, Illinois 60439, USA
[d] Department of Chemical and Biomolecular Engineering, University of Tennessee, Knoxville, Tennessee 37996, USA
[e] Materials Science and Technology Division, Oak Ridge National Laboratory, Oak Ridge, Tennessee 37831, USA

The scalability of the SPEAR method is supported by the fact that vacuum thermal evaporation is an established technique for large-scale production of parts requiring thin coatings for various mechanical, optical, electrical, or chemical properties.[11–13] In the specific context of energy storage, this method is already utilized for lithium metal anode production in commercial thin-film microbatteries, and prototype-level equipment for producing evaporated lithium reels for larger cells is currently available.[14] One drawback of vapor-based methods is the requirement for high-vacuum systems, which can involve significant investment and maintenance costs. However, the SPEAR process does not involve any post-processing (*e.g.* solvent washing or drying steps required by traditional electrochemical prelithiation methods) which serves as a significant trade-off in cost and complexity when considering scalability. By eliminating hazardous waste streams and energy-intensive drying phases, the reproducibility and 'dry' nature of SPEAR present a viable pathway toward industrially relevant battery manufacturing.

When prelithiating using the SPEAR method, increasing the prelithiation amount decreases the open circuit potential (V_{OC}) in line with the standard potential of Li_xSi phases.[10] We hypothesized that exposure of these low V_{OC} electrodes to the electrolyte would change the extent and concentration of reduced electrolyte species to form the SEI, compared to traditional electrochemical approaches. For example, under galvanostatic conditions, electrolyte components are sequentially reduced based on their individual reduction potentials; FEC is reduced at $\sim$1.3 V while EC is at $\sim$1.1 V, leading to a SEI that is dominated by FEC.[15] Thus, FEC additives produce a LiF rich SEI;[16–18] conversely, its absence leads to a more carbonate-like SEI, depicted in Fig. 1a.[19–22] In contrast, SPEAR results in electrodes with a low starting open circuit potential ($<$ 0.5 V), enabling simultaneous reduction of multiple electrolyte species to form the SEI. Furthermore, beyond the reduction potential the concentration of Li within the SPEAR will contribute to a reservoir of highly reducing Li species which will enhance the extent of reaction. Within this lower potential range, EMC could reduce alongside FEC and EC to form more organic SEI components such as lithium methoxide ($LiOCH_3$) and lithium ethoxide ($LiOC_2H_5$), as the reduction potential is $\sim$700 mV *vs.* $Li^{+/0}$ (Fig. 1b).[22,23] Additionally, at low potentials $LiPF_6$ reduction can form LiF as primary degradation product.[24,25] This can cause an increase in the inorganic component contribution to the SEI for highly prelithiated electrodes, as $LiPF_6$ can favorably reduce to form LiF much quicker during the SEI formation process than FEC.

It is hypothesized that these changes in decomposition pathway can lead to the SEI being more robust, and less prone to dissolution over extended periods of time, resulting in improved CE and cycle life. To have predictive understanding on improving SEI cycle life, we first need to relate how SEI composition is affected by prelithiation method and amount. Herein, we report on the difference in SEI chemistry between traditional electrochemical lithiation of electrode architectures (ECLAR) and SPEAR as a function of lithiation degree. We relate these differences to the initial V_{OC} and coulombic efficiency, and total reversible charge capacity after 20 cycles. SEI changes as a function of amount prelithiated were investigated using ^{7}Li and ^{29}Si cross-polarization NMR. SPEAR prelithiated to $Li_{1.38}Si$ yielded a SEI with the most inorganic composition of 71.4% and residual Li decomposition products at the SEI surface. $Li_{0.82}Si$ SPEAR cells exhibited the highest specific capacity at 2941 mAh g^{-1} after SEI formation, suggesting the $Li_{0.28}Si$–$Li_{0.82}Si$ SEIs enable improved Li transport.

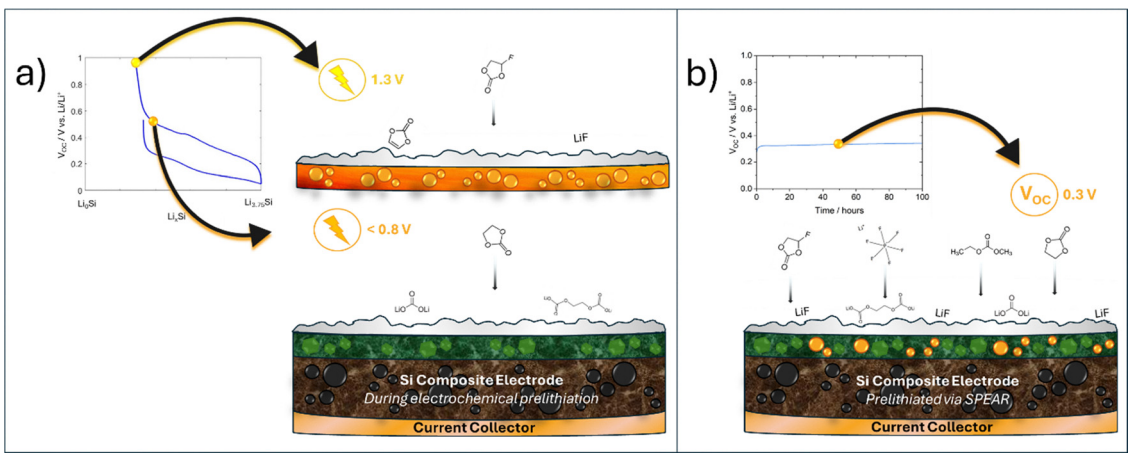

Fig. 1 Schematic diagrams shown next to voltage profiles to depict differences in SEI formation between SPEAR and traditional electrochemical prelithiation processes. (a) A schematic diagram showing reduction of species systematically using electrochemical prelithiation approaches, determined by the reduction potential at which the cell is cycled. FEC could reduce first to form vinylene carbonate and LiF at the electrode surface, followed by reduction of EC to form lithium ethylene dicarbonate (LEDC) and Li_2CO_3. (b) A schematic diagram showing reduction of species stochastically in SPEAR prelithiated electrodes, as the open circuit potential is $<$ 0.5 V and permits favorable reduction of whatever electrolyte species is closest to the electrode surface. This can lead to a more inorganic SEI composition than seen in electrochemical prelithiation, where EMC could reduce stochastically alongside FEC and EC to form lithium methoxide ($LiOCH_3$) and lithium ethoxide ($LiOC_2H_5$), and $LiPF_6$ reduction can form LiF much quicker as the primary degradation product.

2. Experimental section

2.1. Electrode fabrication and prelithiation

Si anodes and NMC 811 cathodes were fabricated at Argonne National Laboratory's Cell Analysis, Modeling and Prototyping (CAMP) Facility. For Si electrodes, slurries were cast on Cu foil with a composition of 80 : 10 : 10 milled Si : polyimide (P84) binder : carbon black. Specifications for the Si electrodes have been previously reported.[9] Electrodes were punched prior to curing at 350 °C for 1 hour under argon (15 mm, 1.77 cm^2 area, mass loading 0.95 mg cm^{-2}, areal capacity 2.0 mAh cm^{-2}). NMC811 cathode slurry was cast with a composition of 90 : 5 : 5 $LiNi_{0.8}Mn_{0.1}Co_{0.1}O_2$ (NMC 811) : C45 carbon black : poly(vinylidene fluoride) (PVDF) binder on aluminum foil before drying under vacuum and punched into electrodes (14 mm, 1.54 cm^2, areal capacity 2.59 mAh cm^{-2}). For consistency, the N/P ratios for all full cells were confined to 0.8 based on areal capacities. Overcharge was averted due to initial losses to form the SEI and capacity available at Si at lower potentials. The N/P ratio was calculated based on the expected reversible capacity for the Si electrodes (between 0.05 and 0.7 V *vs.* Li/Li^+) and under the confines of a 3–4.2 V cycling window for the full cell.

Prelithiation *via* SPEAR was done by thermal evaporation of Li onto Si electrode surfaces under high vacuum ($<10^{-7}$ torr) where it reacted to form Li_xSi.[9,10] A quartz crystal microbalance (QCM) was used to determine the deposition rate to ensure composition control and reproducibility. After prelithiation, the electrodes were transferred into a glovebox with a 96% argon, 4% CO_2 gas mixture environment, where CO_2 was permitted to form a Li_2CO_3 passivation layer at the electrode surface.

2.2. Characterization of prelithiated electrodes

Solid-state NMR was performed on prelithiated and cycled Si anode samples. Samples were harvested from the disassembled coin-cells and packed into either 1.3 mm or 3.2 mm zirconia rotors inside an Ar-filled glovebox (< 0.1 ppm O_2 and < 0.5 ppm H_2O). All NMR measurements were performed on a 500 MHz (11.7 T) Bruker Avance III spectrometer. ^{29}Si solid echo and ^{1}H–^{29}Si cross polarization (CP) experiments were measured for the samples using the 3.2 mm rotors: recycle delays used were 2 s and contact time was 4 ms for ^{1}H–^{29}Si CP experiments. Rotors were spun at a MAS rate of 20 kHz. The ^{7}Li spectra were collected using 1.3 mm zirconia rotors. Solid echo pulse sequences were used. Rotors were spun at 50 kHz. The recycle delays were 15 s and 2 s respectively.

X-ray photoelectron spectroscopy (XPS) was done using a Thermo Scientific (Waltham, MA, USA) Model K-Alpha instrument to study the surface composition of SEIs on Si electrodes as a function of the amount prelithiated using SPEAR. All spectra were obtained using Al Kα X-rays (1486.6 eV) with a 400 μm dia. X-ray spot size. Electrode samples were prepared by prelithiating $Li_{0.28}Si$, $Li_{0.55}Si$, $Li_{0.82}Si$, $Li_{1.10}Si$, and $Li_{1.38}Si$ before cycling in a full cell at C/20 for 3 cycles. For comparative purposes, Si electrodes were also prelithiated using ECLAR to $Li_{0.28}Si$, $Li_{0.82}Si$, $Li_{1.38}Si$, and $Li_{2.33}Si$ ($\sim Li_7Si_3$) to compare SEI compositional differences based on starting V_{OC}. Upon cell disassembly, electrodes were recovered and dipped in dimethyl carbonate (DMC). All samples were loaded in a vacuum transfer holder in a dryroom environment (dew point < −60 °C) to minimize exposure to humidity prior to analysis. During all data collection, the base pressure in the analysis chamber was 2×10^{-9} mbar. A wide energy range survey spectrum (0–1350 eV) was initially acquired to determine all elements present (Fig. S1). Subsequently, a set of narrow energy range core level spectra was acquired for each identified element by using an analyzer pass energy of 200 eV with 1 eV step size. Thermo Scientific Avantage XPS software package (v 4.61) was used to collect data, where the C 1s core level peak at 284.4 eV was used for charge correction. SpecsLab Prodigy was used for data processing.

2.3. Electrochemical methods

A Maccor Series 4000 test system was used for all battery cycling experiments. Coin cells were assembled in an argon-filled glovebox and held at V_{OC} for 4 hours to enable sufficient electrode and separator wetting before cycling. All full cell builds were comprised of Si|NMC811 with Celgard 2325 as the separator and 1.2 M $LiPF_6$ in 3 : 7 (by wt) ethylene carbonate (EC) : ethylmethyl carbonate (EMC) as the electrolyte. Fluoroethylene carbonate (FEC) (3 wt%) was used as an additive due to its role in improved Si anode cycle life.[33] Herein, the electrolyte will be referred to as (GenF3). The acting anode was the Si electrode on Cu foil (15 mm diameter, 1.77 cm^2) at either a pristine (Li_0Si) or prelithiated (Li_xSi, $0.28 \leq x \leq 1.38$) condition *via* SPEAR. The acting cathode was an NMC 811 electrode (14 mm diameter, 1.54 cm^2). All cells were cycled at a C/20 rate for 3 cycles to permit SEI formation. Subsequently, they were disassembled for characterization or were permitted to continue cycling at C/3 for 100 cycles, followed by C/20 for three final cycles to evaluate the extent of capacity recovery. For SEI formation at V_{OC}, electrodes prelithiated *via* SPEAR were assembled into cells and sat at rest for 100 hours prior to characterization or subsequent cycling.

It is important to note that the kinetic environments for SEI formation differ significantly between the two methods. In the SPEAR process, the SEI forms under an open-circuit condition over a 100-hour period where the rate of formation is largely governed by the spontaneous chemical reaction between the electrolyte and the lithiated electrode surface. In contrast, ECLAR involves galvanostatic control, where an applied current density dictates the rate of lithium insertion and, consequently, the potential-dependent breakdown of electrolyte species.

Consequently, the SEI of each prelithiation approach forms under different kinetic regimes, where in SPEAR cells formation is diffusion-limited while formation in ECLAR cells is field-driven. This likely results in distinct SEI interfacial impedances. While the 100-hour V_{OC} rest in SPEAR was intended to ensure complete stochastic SEI formation and equilibration of the potential, the lack of an applied field during this process may result in a more porous or chemically distinct SEI compared to the more compact layers typically formed under active cycling. Furthermore, it is important to distinguish that there is a fundamental difference in how these approaches drive SEI formation.

Electrochemical Impedance Spectroscopy (EIS) experiments were conducted on a Solartron analytical 1400 cell test system fitted with a frequency response analyzer over a range of 10^6–10 Hz. Cells prepared for impedance analysis were obtained from disassembly of Li || Si half cells, and subsequent reassembly as Si//Si symmetric cells.

3. Results and discussion

3.1. Using open circuit potential (V_{OC}) and NMR to study SEI changes in SPEAR electrodes

Because of the high chemical activity of metallic Li reacting with Si to form Li–Si intermetallics, the SPEAR electrodes are expected to exhibit more negative open circuit potentials as a function of amount prelithiation ($Li_{0.28}Si$, $Li_{0.82}Si$, and $Li_{1.38}Si$), which will directly influence the electrolyte species capable of undergoing reduction over time. The SPEAR electrodes were assembled in half cells using GenF3 electrolyte and the V_{OC} was monitored as a function of time (Fig. 2a). The initial V_{OC} observed for $Li_{0.28}Si$ was ~3 V and it decreases as the amount of Li increases to 0.68 and ~0.28 V for $Li_{0.82}Si$ and $Li_{1.38}Si$, respectively. This confirms solid state alloying behavior from the electrodes as more Li reservoir is introduced, forming lithium silicide compositions with low reduction potentials. This is supported by ^{7}Li NMR (Fig. 2b), where the $Li_{0.28}Si$, $Li_{0.82}Si$ and $Li_{1.38}Si$ electrodes underwent spontaneous SEI formation within cells. A shoulder peak at 15 ppm in the normalized spectra can be observed and increases as a function of amount prelithiation, attributed to greater Li transport into the silicon due to more Li inventory from SPEAR to form more Li-rich Li_xSi. Notably, the V_{OC} increases in all SPEAR prelithiated electrodes by 0.1 to 0.5 V before stabilizing with minimum change over the proceeding 90 hours. This suggests Li from SPEAR is active and available to reactively form a SEI.

Ex situ ^{29}Si cross-polarization NMR reveals the signal intensity at −98.32 ppm increases as the amount prelithiated through SPEAR increases (Fig. S2), supporting the formation of a thicker SEI with improved Li transport. As cross-polarization measurements transfer the magnetization *via* heteronuclear dipolar interactions (through-space interactions), a greater amount of ^{1}H is observed in proximity to Si as the amount prelithiated increases, likely indicative of increased EC and EMC reduction products. However, the species are likely smaller molecular weight and are easily removed with washing for XPS preparation, leaving the observed inorganic SEI.

3.2. Chemical considerations: compositional variation of the SEI dependent on prelithiation method and amount prelithiated

We compared the SEI formation between traditional electrochemical lithiation and SPEAR as a function of prelithiation amounts. Here, the SPEARs were permitted to sit at V_{OC} for 100 hours in GenF3-containing half cells before cycling. (Fig. 2a). The electrochemical series were made by lithiating the same Si-based composite electrodes in GenF3 to the targeted stoichiometric prelithiation amounts $Li_{0.28}Si$, $Li_{0.81}Si$, $Li_{1.38}Si$, and $Li_{2.33}Si$ using constant current. The latter stoichiometry was chosen as a direct comparison to the Li_7Si_3 phase reported in previously.[26–29]

The dQ/dV profiles for the first charge step in both cells provide evidence of the different SEI formation mechanisms, where the first charge step for ECLAR was during electrochemical prelithiation, and the first charge step for SPEAR was the first charge after holding at V_{OC} to enable stochastic SEI formation (Fig. S3). In the ECLAR cell, we observe dQ/dV features between 2.5 V and 3.4 V. These correspond to sequential reduction of electrolyte species, specifically FEC (1.2 V *vs.* Li/Li$^+$) and EC (0.8 V *vs.* Li/Li$^+$). On the other hand, the SPEAR cell shows a completely flat baseline with zero capacity contribution in this region. This confirms that the electrolyte reduction processes were completed during the 100-hour V_{OC} rest period prior to the first electrochemical charge in the SPEAR cell.

Additionally, the peak associated with lithiation of Si occurs at a lower cell voltage in the SPEAR cell (3.5 V) than in the

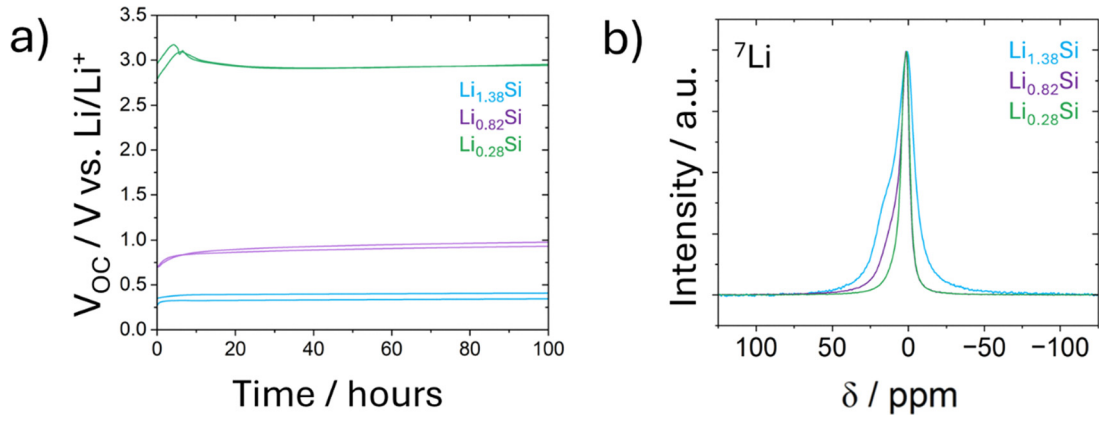

Fig. 2 (a) V_{OC} as function of time for half cells prelithiated to $Li_{0.28}Si$, $Li_{0.82}Si$, and $Li_{1.38}Si$. The cells were assembled and held at V_{OC} for 100 hours to form a reactively formed SEI. (b) Normalized ^{7}Li NMR spectra for Si electrodes prelithiated using SPEAR to $Li_{0.28}Si$, $Li_{0.82}Si$, and $Li_{1.38}Si$ after cycling in a full cell at C/20 for 3 cycles to permit SEI formation, where a shoulder peak at 15 ppm can be observed and increases as a function of amount prelithiated, suggesting the presence of a more Li-rich Li_xSi. The peak at 0 ppm corresponds to residual Li from electrolyte salt and SEI components.

ECLAR cell ($>$ 3.6 V). This shift is due to reduced overpotential in the SPEAR cell, as the surface is already passivated by the stochastically formed SEI. On the other hand, the ECLAR cell must simultaneously build the SEI and initiate lithiation, leading to higher kinetic polarization.

Tables S1 and S2 summarize the SEI surface composition for each prelithiated electrode and was measured by integrating the peaks in the survey spectra to calculate percentages (Fig. S1). All SPEAR prelithiated electrodes have 1% or less Si composition, suggesting that the SEI is greater than 10 nm in thickness (Table S1). Likewise, the Si composition for the ECLAR cells are also $<$ 1%, with the exception of $Li_{0.28}Si$ where the Si composition is 3.3% (Table S2). This suggests that the electrochemical method requires a greater lithiation state to produce a better adhered or thicker SEI.

Assuming the P and F signals report on inorganic SEI components, and the C and O report on the organic, we can graphically depict organic vs inorganic makeup (Fig. 3). It is clear the nature of the insoluble SEI (organic *vs.* inorganic) is highly dependent on the prelithiation method. The ECLAR electrodes are 75.1 to 95.1% organic and 24.9 to 4.9% inorganic. The reduction of species in the electrolyte is selective and dependent on the reduction potential. FEC and EC have higher reduction potentials compared to $LiPF_6$ and EMC, and would furthermore be reduced first at $\sim$1.1 V and $\sim$0.7 V *vs.* Li/Li^+, respectively, to form species such as lithium ethylene dicarbonate (LiEDC) and Li_2CO_3.[30–32] The selective reduction of EC prior to $LiPF_6$ and EMC may also enable the formation of longer, insoluble polymeric chains at the electrochemical SEI surface.

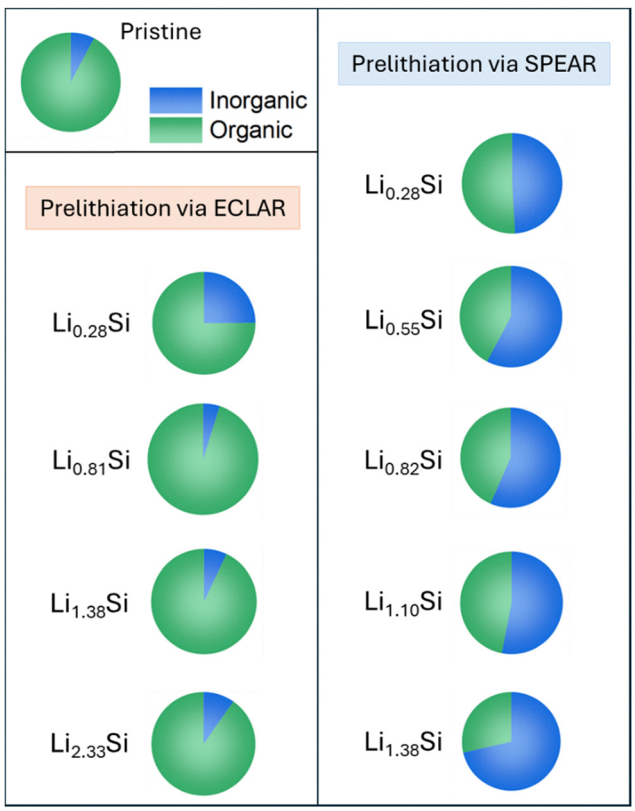

Fig. 3 Pie charts showing surface composition of the SEI formed during electrochemical prelithiation to varying Li_xSi amounts *versus* formation of a reactively formed SEI holding at V_{OC} for 100 hours in SPEAR prelithiated electrodes to varying Li_xSi amounts. Note this is a simplified depiction of the inorganic *versus* organic composition of the insoluble SEI, assuming a majority of the P and F components of the SEI are inorganic, and the C and O components are organic.

The SEI composition of the SPEAR electrodes ranges from 28.6 to 50.9% organic and 71.4 to 49.1% inorganic. The SEI chemistry is not dependent on selective reduction of electrolyte species but is rather driven by simultaneous reduction of EC, EMC, and $LiPF_6$ due to cells having a starting open circuit potential $<$ 0.5 V.[10] This is a competitive process in which the species reduced is largely dependent on what component is closest to the electrode surface and available to undergo reduction. As a result, the surface speciation across electrode SEIs is drastically different, determinate on the prelithiation method used. For SPEAR electrodes, $LiPF_6$ is reduced to begin PO_x and $LiPF_x$ formation immediately, causing the formation of a more inorganic SEI with greater PO_x, LiPFx, and LiF composition in the SEI (as LiF is a primary degradation product from $LiPF_6$ reduction). Additionally, simultaneous EC/EMC reduction likely results in shorter lithium alkyl carbonate chains, which could be more susceptible to being washed away during the DMC rinse step prior to XPS.[10]

When comparing the inorganic and organic components individually (P and F *vs.* C and O composition, respectively), the inorganic SEI component of all SPEAR electrodes is F enriched and could improve electrochemical cycling. In fact, electrochemical prelithiation beyond a stoichiometry of $Li_{0.28}Si$ results in negligible P present in the SEI and a decrease in F to 9.2%. This suggests there is more SEI formation from $LiPF_6$ salt reduction than FEC reduction in the SPEAR prelithiated electrodes to form a SEI with more PO_x and $LiPF_x$ content, whereas less reduction of $LiPF_6$ and FEC is observed in ECLAR electrodes. However, the amount of FEC reduction observed in ECLAR electrodes is significantly higher than $LiPF_6$ reduction, as evidenced by the lack of P in the SEI. This argument can be supported by the F 1s spectra, where the feature at 686.1 eV corresponding to $LiPF_x$ is greater in intensity in SPEAR electrodes compared to ECLAR electrodes (Fig. 4 and 5b) relative to the LiF peak at 683.7 eV. Additionally, the peak at 533.8 eV in the O 1s spectra for SPEAR electrodes corresponds to PO_x formation, which is absent in the SEI of all ECLAR electrodes (Fig. 4 and 5c). Further, the electrochemical prelithiation resulted in SEI of much more organic composition, with up to a 21% increase in C and 45% O observed, compared to SPEAR electrodes (Fig. S4). This is largely due to the significant amount of CO_3 detected in the C 1s spectra for ECLAR SEIs at 290.0 eV, which is absent in the SEI of all SPEAR electrodes (Fig. 4 and 5a).

Conclusively, the SEI surface composition can be controlled by prelithiation method. SPEAR results in a SEI with greater PO_x, LiPFx, and LiF composition, as well as shorter lithium alkyl carbonate chains resulting in a primarily inorganic insoluble SEI. Electrochemical lithiation shifts the insoluble SEI composition to more organic-like consisting of CO_3-type moieties.

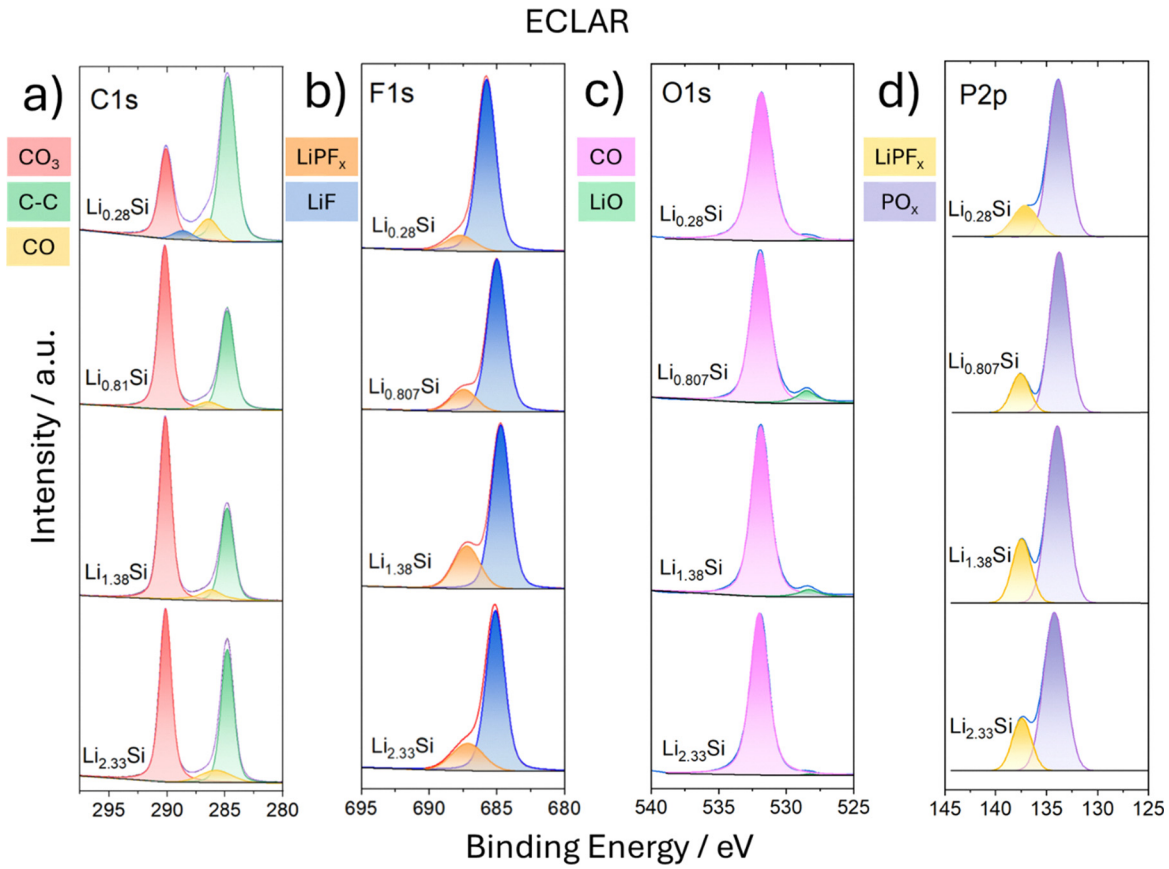

Fig. 4 (a) F 1s, (b) P 2p, (c) C 1s, and (d) O 1s XPS spectra of Si-based composite electrodes which have been prelithiated *via* ECLAR to $Li_{0.28}Si$, $Li_{0.81}Si$, $Li_{1.38}Si$, and $Li_{2.33}Si$ stoichiometries. All ECLAR electrodes were prepared by discharging half cells at C/20 to Li_xSi, enabling SEI formation, before cell disassembly. All electrodes were rinsed in DMC prior to XPS analysis. Species are defined and color coordinated to the left of each respective spectra.

These differences in surface speciation are expected to impact cycling performance *via* changes in Li transport and homogeneity of speciation across the SEI surface.

3.3. Electrochemical considerations: changes in impedance spectroscopy as a function of prelithiation method and amount

After SEI formation, cells were disassembled and reassembled into symmetric cells to collect electrochemical impedance spectroscopy (EIS) at 3.0 V to isolate and study solely the electrochemical impedance of the prelithiated electrode. The impedance of ECLAR *vs.* SPEAR symmetric cells were compared to understand the differences in Li transport through the SEI and porous structure (Fig. 6). Corresponding equivalent circuit models and fit values for each Nyquist plot can be found in Fig. S5 and Table S3. For all ECLAR cells, the semicircle at high to medium frequencies can be attributed to SEI resistance (R_{SEI}) and decrease in magnitude as the extent of prelithiated increases (Fig. 6a). This is due to the formation of a thicker, more robust SEI at greater prelithiation amounts (consistent with XPS). Indeed, previous EIS studies for thermally evaporated Si anodes also show a 3875 Ω decrease in charge transfer resistance and 162 Ω decrease in SEI resistance as the prelithiation amount increases to $Li_{4.4}Si$.[10]

The 45° slope is observed at low frequencies for the $Li_{1.38}Si$ ECLAR cells, characteristic of diffusion/mass transport limitation and suggesting either restrictive transport through the SI pores (Si particle growth may decrease pore size) or the Li transport through the SEI lined pore walls becomes limiting (Fig. 6a).[33,34] During the SEI formation process, all ECLAR cells undergo the same electrochemical lithiation process to systematically reduce organic species (*e.g.* FEC at ~1.1 V *vs.* Li/Li^+; EC at ~0.7 V *vs.* Li/Li^+) first. This results in SEI compositions that look consistent in their surface speciation across all ECLAR cells, independent of amount prelithiated.

Interestingly, the Nyquist plots for the SPEAR method exhibit a slope before takeoff at mid-frequencies with an angle ~22.5° (Fig. 6b). This can be attributed to changes in porosity due to closing pores or having Li-rich and Li-poor pores that result in an effective multipore structure. Such pore reduction occurs during the thermal evaporation process, where the extent of porosity is reduced due to lithium silicide formation and expansion of Si by 32.7%, confirmed using PFIB-SEM in previous work.[10] As supported by the V_{OC} during SEI formation and XPS data, the starting potential of SPEAR cells decreases to < 0.3 V for cells prelithiated to $Li_{1.38}Si$. This enables competitive reduction of multiple species to form a mostly inorganic phase SEI due to $LiPF_6$ and FEC reduction through the growth of surface passivation. Additionally, electrolyte can fill the pores where it can readily react with Li_xSi. This reduces the number of

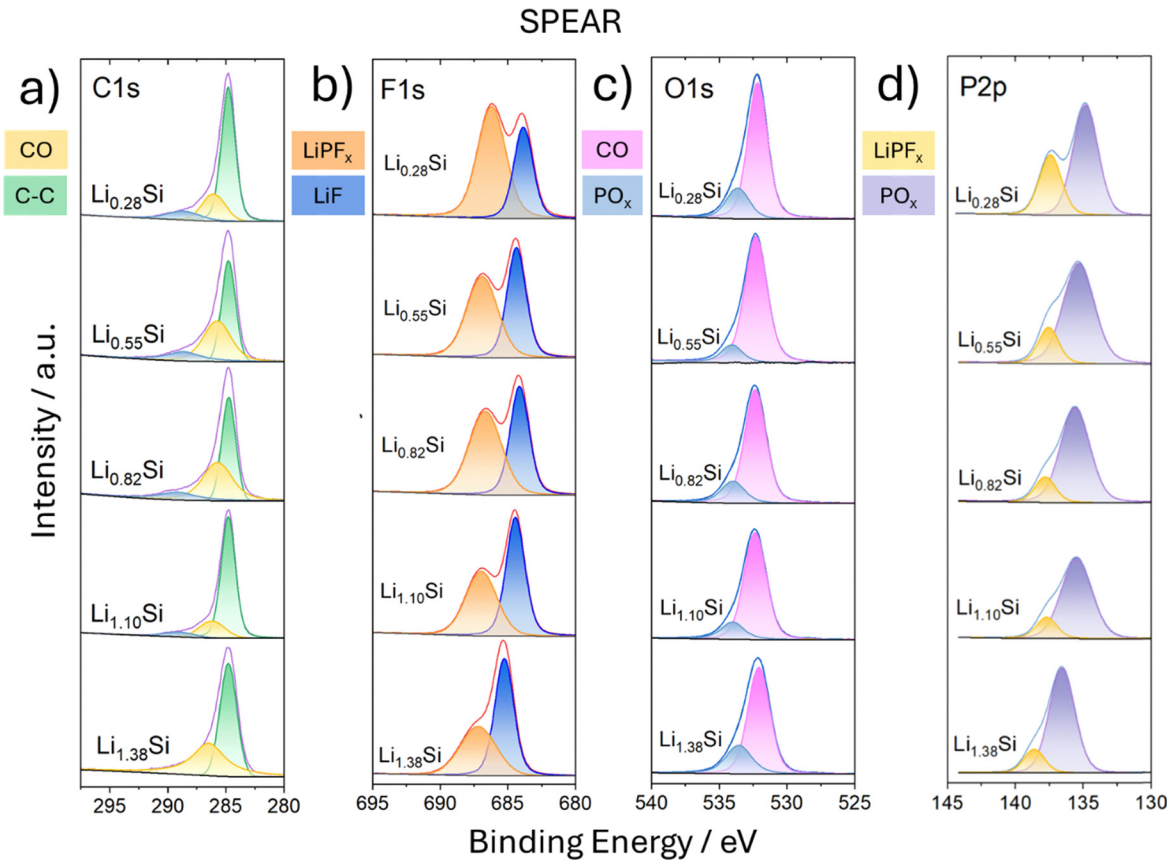

Fig. 5 (a) F 1s, (b) P 2p, (c) C 1s, and (d) O 1s XPS spectra of Si-based composite electrodes which have been prelithiated using the SPEAR technique to $Li_{0.28}Si$, $Li_{0.55}Si$, $Li_{0.82}Si$ $Li_{1.10}Si$, and $Li_{1.38}Si$ stoichiometries. To study compositional changes in SEI as a function of amount prelithiated *via* SPEAR, all electrodes were assembled into full cells and cycled for 3 formation cycles at C/20. All cells were disassembled and the electrodes were rinsed in DMC prior to XPS analysis. Species are defined and color coordinated to the left of each respective spectra.

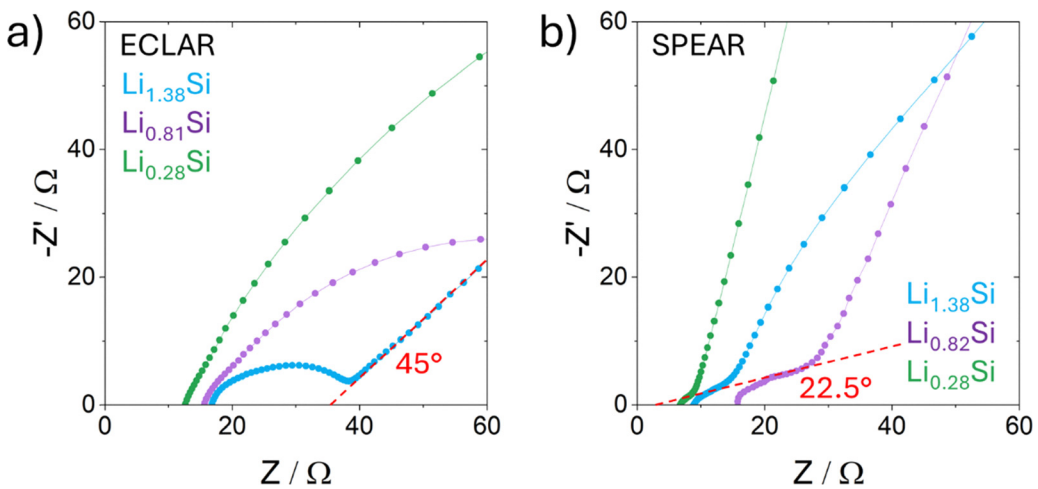

Fig. 6 Nyquist plots for symmetric cells prelithiated using (a) ECLAR *vs.* (b) SPEAR. Note the difference in the slope angle at low frequencies (45° for electrochemical prelithiation to $Li_{1.38}Si$; 22.5° for SPEAR prelithiated electrodes), suggesting diffusion-limited bulk mass transport and larger pores throughout the ECLAR electrodes in the low frequency region, and pore reduction resulting from Li_xSi formation in SPEAR prelithiated electrodes in the mid frequency region.

Li environments available and decreases the overall high frequency impedance to 9 Ω to more closely resemble the $Li_{0.28}Si$ cell (7 Ω) than the $Li_{0.82}Si$ cell (16 Ω). As a result, SPEAR results in lower SEI and charge transfer impedance. These mechanisms are different than that which is observed in ECLAR cells, where the porosity of the electrode is not decreased prior to cycling the

cell to form Li_xSi. In this instance, pores are filled with electrolyte and remain unreacted until electrochemical cycling begins where a SEI is formed at the surface and lithium silicide formation is electrochemically driven. However, the difference in these solution resistances is not significant enough to expect impact on electrochemical performance.

3.4. Improvements in initial coulombic efficiency (ICE) and formation cycling in prelithiated cells

To study whether or not changes in electrochemical SEI formation are observed as a function of prelithiation amount in SPEAR cells, a series of full cells were built using Li_xSi (x = 0 − 1.38) and cycled at C/20 for 3 cycles, permitting full Si utilization and to enable any additional SEI formation electrochemically after formation of a SEI reactively, before continued C/3 cycling. The initial coulombic efficiency (ICE) of the cells increases as a function of amount prelithiated (Fig. 7a). Similar behavior is observed after cycles 2–3, where the CE continues to improve significantly, quickly approaching 100%. Interestingly, the $Li_{1.38}Si$ full cell approaches 99.4% CE by cycle 2, whereas the Li_0Si full cell only reaches 96.0% CE by the third formation cycle. This suggests a faster SEI formation process in ECLAR cells, as a large component of the SEI has already undergone formation reactively to yield a more optimal SEI. However, an additional SEI component may form electrochemically during the initial cycle which could explain the 82% ICE observed for $Li_{1.38}Si$.

Improvements in ICE during SEI formation are incommensurate to the extent of prelithiation, depicted by the trend observed in Fig. 7 where an 11.7% improvement is observed between Li_0Si and $Li_{0.55}Si$, and only a 4.5% improvement prelithiating up to $Li_{1.38}Si$. In fact, ICE as a function of amount prelithiated (Fig. 7b) fits to an exponential function (R^2 = 0.996) as expressed in eqn (1), where a is the CE_0 of base Si anode, b is the exponential factor, x is the stoichiometric amount of Li in the prelithiated electrode, and t is time which can be directly correlated to cycle number. As x increases, a "maximum" ICE is observed where very small improvements are observed at $x >$ 0.82. Conclusively, a 19.6% improvement is observed when comparing $Li_{1.38}Si$ full cells to its Li_0Si counterpart which shows Li is compensating for losses to SEI formation.

$$\mathrm{ICE} = a + be^{\frac{-x}{t}} \quad (1)$$

This suggests that the ICE cannot reach 100% for these cells due to cathode limitations depending on the electrodes used and potential limits. In fact, 6–17% irreversibility is commonly reported for NMC811 half cells.[35,36] Rather, a maximum ICE of 82% is observed for $Li_{1.38}Si$ as Li may participate during the first formation cycle to form additional SEI, and cathode irreversibility is inevitable. Negligible changes in transport may also be due to limitations in starting V_{OC}; once electrodes are prelithiated beyond $Li_{0.82}Si$, changes in the starting V_{OC} become less prominent and stochastic reduction of electrolyte species begins to look similar across electrodes prelithiated to $Li_{0.82}Si$, $Li_{1.10}Si$, and $Li_{1.38}Si$.

While the CE is directly proportional to the amount prelithiated, the specific capacity observed during SEI formation cycling is not (Fig. 8). A C/20 rate was used for the first three SEI formation cycles, followed by C/3 cycling for continual exercising of the silicon up to 20 cycles. The focus remains on the performance during the first 20 cycles, as it captures the immediate impact of SPEAR and ECLAR on the reversible lithium inventory. As x increases to 0.82, an increase in initial specific capacity up to 2941 mAh g^{-1} (Fig. 8a and b) is observed, compared to ~2750 mAh g^{-1} for its base Li_0Si counterpart. Surprisingly, at $x > 0.82$, the initial specific capacity gradually declines from 2941 to 2827 mAh g^{-1} at $Li_{1.38}Si$, respectively, revealing an apparent "Goldilocks sweet spot." The identification of an optimal prelithiation level at $Li_{0.82}Si$ to maximize initial specific capacity suggests a critical balance between compensating for first-cycle loss and maintaining the mechanical integrity of the electrode. While the specific causes of degradation at higher prelithiation amounts are not directly decoupled here,

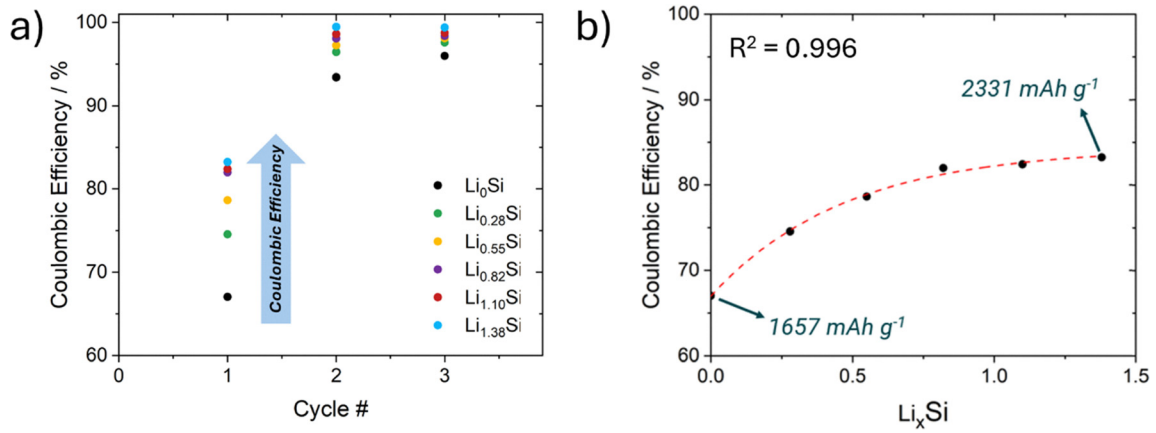

Fig. 7 (a) CE of Si full cells prelithiated *via* SPEAR to Li_xSi (x = 0.28 − 1.38) compared to a nonprelithiated Si full cell during the first three SEI formation cycles, carried out using a C/20 rate. Note the ICE increases as a function of amount prelithiated, and the CE reaches 100% quicker over the course of formation cycling as amount prelithiated increases. (b) ICE plotted as a function of amount prelithiated, which can be fit to an exponential function suggesting the maximum ICE permissible is 82%.

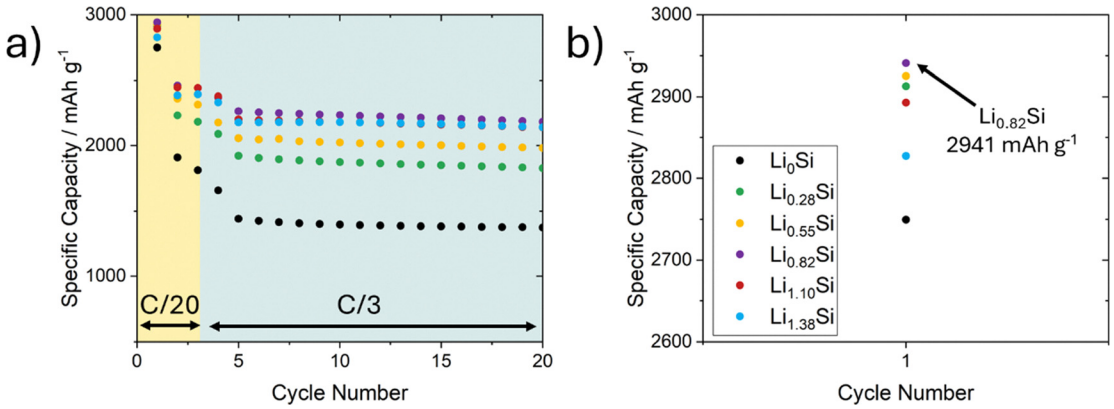

Fig. 8 (a) Specific capacity (charging step) as a function of cycle number for Li_xSi full cells (x = 0 to 1.38) for the SEI formation cycles at C/20 before subsequent C/3 cycling. The cathode used was NMC 811 (N/P = 0.8), the separator was Celgard 2325, and the electrolyte was GenF3. (b) A zoomed-in view of the specific capacity for Li_xSi full cells (x = 0 to 1.38) after the first cycle, where $Li_{0.82}Si$ exhibits the highest specific capacity at 2941 mAh g^{-1}.

the drop in capacity beyond $Li_{0.82}Si$ is consistent with the known onset of high stress within the Si lattice. Specifically, as the lithium concentration increases up to $Li_{15}Si_4$, 300% volume expansion has been observed which facilitates Si particle fracturing and continuous exposure of fresh Si surfaces, which accelerates parasitic electrolyte consumption.[37–39] Mechanical stresses have also been previously reported for these systems such that more prelithiation results in higher Si utilization, leading to greater stresses.[9]

Another possible contributing factor could be that at $x > 0.82$, parasitic reactions could increase where an increased favorability for electrolyte decomposition and SEI instability is observed outside the electrolyte's thermodynamic stability window.[40,41] Additionally, excessive reduction of $LiPF_6$ to form LiF and degradation products could begin to increase impedance, and could result in a SEI with less ideal transport properties or stability. The effective voltage window is another determinant variable, as the amount of capacity the electrodes can exchange may be constrained within the voltage cutoffs imposed on the cell.

Conclusively from this study, $Li_{0.82}Si$ appears to be the point where the benefits of excess lithium inventory are maximized before they are offset by kinetic and mechanical limitations *via* excessive expansion. A more extensive analysis of these competing mechanisms would require operando stress or surface-sensitive spectroscopy; however, the electrochemical performance data suggests clear optimization at prelithiation to $Li_{0.82}Si$.

4. Summary and outlook

In contrast to traditional electrochemical prelithiation (where the potential is swept and electrolyte components are reduced based on reduction potentials) prelithiation *via* SPEAR yields defined Li_xSi stoichiometries that begin SEI formation at substantially lower V_{OC}, enabling favorable, stochastic reduction of multiple electrolyte species (*e.g.* EC, EMC, $LiPF_6$), and resulting in the formation of an SEI with different inorganic/organic compositions. EIS revealed SPEAR electrodes exhibited a 22.5° slope in the mid-frequency region, pointing to changes in the pore structure due to Li_xSi expansion upon prelithiation. SPEARs showed a significantly decreased initial V_{OC} from ~3 V at $Li_{0.28}Si$ to < 0.5 V which corresponded to thicker SEI formation and greater Li_xSi formation, supported by ^7Li and ^{29}Si cross polarization NMR *ex situ* studies. At reduction potentials <0.5 V, favorable reduction of multiple species was found to form a mostly inorganic phase SEI due to $LiPF_6$ and FEC reduction. XPS further showed that SPEAR electrodes form a predominantly inorganic insoluble SEI, with a composition up to 71.4% inorganic for $Li_{1.38}Si$ with increased P/F contributions consistent with more extensive $LiPF_6$ reduction to form PO_x, $LiPF_x$, and LiF. On the other hand, ECLAR electrodes exhibited comparatively more organic/carbonate-rich SEI compositions. As a result of these compositional changes observed *via* XPS, electrochemical cycling of SPEAR full cells revealed an improved initial coulombic efficiency (ICE) up to 82%. Negligible changes in ICE and transport are attributed to limitations in the starting V_{OC}, as stochastic reduction of electrolyte species begins to look similar across electrodes prelithiated beyond $Li_{0.82}Si$. The specific capacity exhibited a "Goldilocks zone," where $Li_{0.82}Si$ delivered the highest post-formation specific capacity (2941 mAh g^{-1} during initial cycle), suggesting an optimal SEI chemistry and superior Li transport at intermediate prelithiation amounts.

Conflicts of interest

There are no conflicts to declare.

Data availability

Supplementary information (SI) is available. See DOI: https://doi.org/10.1039/d6ya00065g.

Acknowledgements

This work was supported by U.S. Department of Energy's Transportation Technologies Office under the Silicon Consortium Project, directed by Carine Steinway, Nicolas Eidson,

Thomas Do, and Brian Cunningham, and managed by Anthony Burrell. The electrodes examined in this work are from Argonne's CAMP Facility, which is supported in part by CMEI: the authors thank Stephen Trask for fabricating the electrodes at the CAMP facility. This manuscript has been created by Oak Ridge National Laboratory, managed by UT-Battelle, LLC, for the DOE under contract DE-AC05-00OR22725, Argonne National Laboratory, managed by UChicago Argonne, LLC, for the DOE under contract DE-AC02-06CH11357, and National Laboratory of the Rockies, managed by Alliance for Energy Innovation LLC, for the DOE under contract DE-AC36-08GO28308. The U.S. Government retains for itself, and others acting on its behalf, a paid-up nonexclusive, irrevocable worldwide license in said article to reproduce, prepare derivative works, distribute copies to the public, and perform publicly and display publicly, by or on behalf of the Government.

References

1 J.-H. Trill, C. Tao, M. Winter, S. Passerini and H. Eckert, NMR Investigations on the Lithiation and Delithiation of Nanosilicon-Based Anodes for Li-Ion Batteries, *J. Solid State Electrochem.*, 2011, **15**(2), 349–356, DOI: 10.1007/s10008-010-1260-0.

2 B. Wu, C. Chen, D. L. Danilov, M. Jiang, L. H. J. Raijmakers, R.-A. Eichel and P. H. L. Notten, Influence of the SEI Formation on the Stability and Lithium Diffusion in Si Electrodes, *ACS Omega*, 2022, **7**(36), 32740–32748, DOI: 10.1021/acsomega.2c04415.

3 F. Holtstiege, A. Wilken, M. Winter and T. Placke, Running out of Lithium? A Route to Differentiate between Capacity Losses and Active Lithium Losses in Lithium-Ion Batteries, *Phys. Chem. Chem. Phys.*, 2017, **19**(38), 25905–25918, DOI: 10.1039/C7CP05405J.

4 H. Wu, G. Chan, J. W. Choi, I. Ryu, Y. Yao, M. T. McDowell, S. W. Lee, A. Jackson, Y. Yang, L. Hu and Y. Cui, Stable Cycling of Double-Walled Silicon Nanotube Battery Anodes through Solid–Electrolyte Interphase Control, *Nat. Nanotechnol.*, 2012, **7**(5), 310–315, DOI: 10.1038/nnano.2012.35.

5 X. Zhao, M. Muraleedharan Pillai, N. Kalidas, S. Karuppiah, G. Hernández, D. Brandell and V.-P. Lehto, Electrochemical Prelithiation of Self-Standing Mesoporous Silicon Film Anodes for Enhanced Si‖NMC Full-Cell Performance, *J. Electrochem. Soc.*, 2025, **172**(8), 080512, DOI: 10.1149/1945-7111/adf5ee.

6 S. Bai, W. Bao, K. Qian, B. Han, W. Li, B. Sayahpour, B. Sreenarayanan, D. H. S. Tan, S. Ham and Y. S. Meng, Elucidating the Role of Prelithiation in Si-Based Anodes for Interface Stabilization, *Adv. Energy Mater.*, 2023, **13**(28), 2301041, DOI: 10.1002/aenm.202301041.

7 C. Shen, R. Fu, Y. Xia and Z. Liu, New Perspective to Understand the Effect of Electrochemical Prelithiation Behaviors on Silicon Monoxide, *RSC Adv.*, 2018, **8**(26), 14473–14478, DOI: 10.1039/c8ra01917g.

8 A. V. Bhujbal, K. L. Ng, S. Khazraei, J. Bekou and A. R. Riahi, Recent Advances in Prelithiation of Silicon Anode: Enhanced Strategy for Boosting Practicability of Li-Ion Battery, *J. Electrochem. Soc.*, 2023, **170**(8), 080506, DOI: 10.1149/1945-7111/aceb36.

9 A. L. Musgrove, A. Verma, M.-T. F. Rodrigues, C. I. McDaniel, D. P. Abraham, S. Lam, A. Colclasure, A. Singh, B. L. Armstrong and G. M. Veith, Solid-State Prealkylation of Electrode Architectures (SPEAR): Direct Control of Prelithiation Levels in Silicon Anodes and Electrochemical Cycling, *Adv. Mater. Technol.*, 2025, e02088, DOI: 10.1002/admt.202502088.

10 A. L. Musgrove, K. L. Browning, R. L. Sacci, A. Ullman, H. M. I. Meyer, K. Musgrove, J. Quinn, S. Möller, M. Finsterbusch and G. M. Veith, Direct Prelithiation of Silicon-Based Composite Electrodes via Island-like Thermal Evaporation, *Energy Fuels*, 2025, **39**(10), 4968–4982, DOI: 10.1021/acs.energyfuels.4c06113.

11 D. M. Taylor, Vacuum-Thermal-Evaporation: The Route for Roll-to-Roll Production of Large-Area Organic Electronic Circuits, *Semicond. Sci. Technol.*, 2015, **30**(5), 054002, DOI: 10.1088/0268-1242/30/5/054002.

12 N. Rospars, M. Srout, C. Fu, G. Mourouga, M. Mensi and A. Ingenito, High Performance Ultra-Thin Lithium Metal Anode Enabled by Vacuum Thermal Evaporation, *Commun Mater*, 2024, **5**(1), 179, DOI: 10.1038/s43246-024-00619-9.

13 A. Bashir; T. I. Awan; A. Tehseen; M. B. Tahir and M. Ijaz, Chapter 3 – Interfaces and Surfaces, *Chemistry of Nanomaterials*, Elsevier, 2020, pp. 51–87, ISBN 9780128189085, DOI: 10.1016/B978-0-12-818908-5.00003-2.

14 B. Acebedo, M. C. Morant-Miñana, E. Gonzalo, I. Ruiz de Larramendi, A. Villaverde, J. Rikarte and L. Fallarino, Current Status and Future Perspective on Lithium Metal Anode Production Methods, *Adv. Energy Mater.*, 2023, **13**(13), 2203744, DOI: 10.1002/aenm.202203744.

15 C. Xu, F. Lindgren, B. Philippe, M. Gorgoi, F. Björefors, K. Edström and T. Gustafsson, Improved Performance of the Silicon Anode for Li-Ion Batteries: Understanding the Surface Modification Mechanism of Fluoroethylene Carbonate as an Effective Electrolyte Additive, *Chem. Mater.*, 2015, **27**(7), 2591–2599, DOI: 10.1021/acs.chemmater.5b00339.

16 P. J. Weddle, E. W. C. Spotte-Smith, A. Verma, H. D. Patel, K. Fink, B. J. Tremolet De Villers, M. C. Schulze, S. M. Blau, K. A. Smith, K. A. Persson and A. M. Colclasure, Continuum-Level Modeling of Li-Ion Battery SEI by Upscaling Atomistically Informed Reaction Mechanisms, *Electrochim. Acta*, 2023, **468**, 143121, DOI: 10.1016/j.electacta.2023.143121.

17 T. Hou, G. Yang, N. N. Rajput, J. Self, S.-W. Park, J. Nanda and K. A. Persson, The influence of FEC on the solvation structure and reduction reaction of LiPF6/EC electrolytes and its implication for solid electrolyte interphase formation, *Nano Energy*, 2019, **64**, 103881, DOI: 10.1016/j.nanoen.2019.103881.

18 K. Uta Schwenke, S. Solchenbach, J. Demeaux, B. Lucht and H. A. Gasteiger, The Impact of CO_2 Evolved from VC and FEC during Formation of Graphite Anodes in Lithium-Ion

Batteries, *J. Electrochem. Soc.*, 2019, **166**(10), A2035–A2047, DOI: 10.1149/2.0821910jes.

19 R. Lundström, N. Gogoi, T. Melin and E. J. Berg, Unveiling Reaction Pathways of Ethylene Carbonate and Vinylene Carbonate in Li-Ion Batteries, *J. Phys. Chem. C*, 2024, **128**(20), 8147–8153, DOI: 10.1021/acs.jpcc.4c00927.

20 D. Aurbach, B. Markovsky, A. Shechter, Y. Ein-Eli and H. Cohen, A Comparative Study of Synthetic Graphite and Li Electrodes in Electrolyte Solutions Based on Ethylene Carbonate-Dimethyl Carbonate Mixtures, *J. Electrochem. Soc.*, 1996, **143**(12), 3809, DOI: 10.1149/1.1837300.

21 A. M. Haregewoin, E. G. Leggesse, J.-C. Jiang, F.-M. Wang, B.-J. Hwang and S. D. Lin, Comparative Study on the Solid Electrolyte Interface Formation by the Reduction of Alkyl Carbonates in Lithium Ion Battery, *Electrochim. Acta*, 2014, **136**, 274–285, DOI: 10.1016/j.electacta.2014.05.103.

22 Q. Wu, M. T. McDowell and Y. Qi, Effect of the Electric Double Layer (EDL) in Multicomponent Electrolyte Reduction and Solid Electrolyte Interphase (SEI) Formation in Lithium Batteries, *J. Am. Chem. Soc.*, 2023, **145**(4), 2473–2484, DOI: 10.1021/jacs.2c11807.

23 H.-J. Peng, C. Villevieille, S. Trabesinger, H. Wolf, K. Leitner and P. Novák, Mechanism of the Carbonate-Based-Electrolyte Degradation and Its Effects on the Electrochemical Performance of $Li_{1+x}(Ni_aCo_bMn_{1-a-b})_{1-x}O_2$ Cells, *J. Power Sources*, 2016, **335**, 91–97, DOI: 10.1016/j.jpowsour.2016.10.031.

24 M. Soto, K. Fink, C. Zweifel, P. J. Weddle, E. W. C. Spotte-Smith, G. M. Veith, K. A. Persson, A. M. Colclasure and B. J. Tremolet De Villers, Solubilities of Ethylene and Carbon Dioxide Gases in Lithium-Ion Battery Electrolyte, *J. Chem. Eng. Data*, 2024, **69**(6), 2236–2243, DOI: 10.1021/acs.jced.3c00692.

25 C. Cao, I. I. Abate, E. Sivonxay, B. Shyam, C. Jia, B. Moritz, T. P. Devereaux, K. A. Persson, H.-G. Steinrück and M. F. Toney, Solid Electrolyte Interphase on Native Oxide-Terminated Silicon Anodes for Li-Ion Batteries, *Joule*, 2019, **3**(3), 762–781, DOI: 10.1016/j.joule.2018.12.013.

26 A. Azad, K. Bateman, M. Irvine, A. B. Naden, S. A. M. Dickson, R. I. Smith, R. K. B. Gover and J. T. S. Irvine, Thermal Expansion of Lithiated Silicon ($Li_{13}Si_4$ and Li_7Si_3) Anodes: A Powder Neutron Diffraction Study, *J. Mater. Chem. A*, 2025, **13**(20), 14836–14845, DOI: 10.1039/D4TA07858F.

27 L. C. Loaiza, L. Monconduit and V. Seznec, Si and Ge-Based Anode Materials for Li-, Na-, and K-Ion Batteries: A Perspective from Structure to Electrochemical Mechanism, *Small*, 2020, **16**(5), 1905260, DOI: 10.1002/smll.201905260.

28 M. Zeilinger, V. Baran, L. van Wüllen, U. Häussermann and T. F. Fässler, Stabilizing the Phase $Li_{15}Si_4$ through Lithium–Aluminum Substitution in $Li_{15-x}Al_xSi_4$ ($0.4 < x < 0.8$)—Single Crystal X-Ray Structure Determination of Li15Si4 and $Li_{14.37}Al_{0.63}Si_4$, *Chem. Mater.*, 2013, **25**(20), 4113–4121, DOI: 10.1021/cm402721n.

29 F. Yang, Cycling-Induced Structural Damage/Degradation of Electrode Materials–Microscopic Viewpoint, *Nanotechnology*, 2021, **33**(6), 065405, DOI: 10.1088/1361-6528/ac3616.

30 D. Aurbach, B. Markovsky, A. Shechter, Y. Ein-Eli and H. Cohen, A Comparative Study of Synthetic Graphite and Li Electrodes in Electrolyte Solutions Based on Ethylene Carbonate-Dimethyl Carbonate Mixtures, *J. Electrochem. Soc.*, 1996, **143**(12), 3809, DOI: 10.1149/1.1837300.

31 D. M. Seo, D. Chalasani, B. S. Parimalam, R. Kadam, M. Nie and B. L. Lucht, Reduction Reactions of Carbonate Solvents for Lithium Ion Batteries, *ECS Electrochem. Lett.*, 2014, **3**(9), A91, DOI: 10.1149/2.0021409eel.

32 R. Imhof and P. Novák, In Situ Investigation of the Electrochemical Reduction of Carbonate Electrolyte Solutions at Graphite Electrodes, *J. Electrochem. Soc.*, 1998, **145**(4), 1081, DOI: 10.1149/1.1838420.

33 A. Lasia, Impedance of Porous Electrodes, *J. Electroanal. Chem.*, 1995, **397**(1), 27–33, DOI: 10.1016/0022-0728(95)04177-5.

34 A. Lasia, Impedance of Porous Electrodes in the Presence of Electroactive Species and Solution Resistance, *J. Electroanal. Chem.*, 2023, **951**, 117919, DOI: 10.1016/j.jelechem.2023.117919.

35 R. C. McNulty, E. Hampson, L. N. Cutler, C. P. Grey, W. M. Dose and L. R. Johnson, Understanding the Limits of Li-NMC811 Half-Cells, *J. Mater. Chem. A*, 2023, **11**(34), 18302–18312, DOI: 10.1039/D3TA00912B.

36 H. Zheng, Q. Sun, G. Liu, X. Song and V. Battaglia, Correlation between Dissolution Behavior and Electrochemical Cycling Performance for $LiNi_{1/3}Co_{1/3}Mn_{1/3}O_2$-Based Cells, *J. Power Sources*, 2012, **207**, 134–140, DOI: 10.1016/j.jpowsour.2012.01.122.

37 M. A. Islam, J. Turallo, J. Yang and S.-D. Han, Suppression of Crystalline $Li_{15}Si_4$ in Silicon-Carbon Composite Anode with a Co-Polymer Binder for Lithium Ion Batteries, *J. Power Sources*, 2025, **641**, 236742, DOI: 10.1016/j.jpowsour.2025.236742.

38 H. Zhang, Y. Su, Y. Chen, F. Liu, R. Zhu, P. Zhao, L. Wei, W. Li, T. Chen and J. Fu, Insights into the Structure–Property–Function Relationships of Silicon-Based Anode Binders for Lithium-Ion Batteries, *Ind. Eng. Chem. Res.*, 2024, **63**(49), 21125–21145, DOI: 10.1021/acs.iecr.4c02837.

39 T. Kwon, J. W. Choi and A. Coskun, The Emerging Era of Supramolecular Polymeric Binders in Silicon Anodes, *Chem. Soc. Rev.*, 2018, **47**(6), 2145–2164, DOI: 10.1039/C7CS00858A.

40 B. Aktekin, L. M. Riegger, S.-K. Otto, T. Fuchs, A. Henss and J. Janek, SEI Growth on Lithium Metal Anodes in Solid-State Batteries Quantified with Coulometric Titration Time Analysis, *Nat. Commun.*, 2023, **14**(1), 6946, DOI: 10.1038/s41467-023-42512-y.

41 K. Xu, Electrolytes and Interphases in Li-Ion Batteries and Beyond, *Chem. Rev.*, 2014, **114**(23), 11503–11618, DOI: 10.1021/cr500003w.